Dalton Transactions

PAPER

Cite this: *Dalton Trans.*, 2015, **44**, 6863

Isoquinoline-based Werner clathrates with xylene isomers: aromatic interactions *vs.* molecular flexibility†

Merrill M. Wicht,[a,b] Nikoletta B. Báthori*[b] and Luigi R. Nassimbeni[a]

Received 8th January 2015,
Accepted 4th March 2015

DOI: 10.1039/c5dt00084j

www.rsc.org/dalton

The crystal structures of the Werner clathrates $Ni(NCS)_2(isoquinoline)_4$ (**H**) with *para*-xylene (**px**), *meta*-xylene (**mx**) and *ortho*-xylene (**ox**) have been elucidated. The kinetics of thermal decomposition of the three inclusion compounds were performed using the isothermal technique of Flynn and Wall. Selectivity of **H** for the xylene isomers was determined for both the liquid and vapour phase binary mixtures of the xylenes. The chosen ligand has a larger aromatic system to improve the possible π interactions between **H** and the selected guests. The planarity of the isoquinoline ligand causes **H** rigidity and its selectivity was compared to a related Werner complex containing the more flexible 4-phenylpyridine.

Introduction

Werner clathrates are inclusion compounds of general formula $MX_2L_4{\cdot}nG$, where M is a divalent metal cation (typically Ni(II), Co(II), Fe(II), Cu(II) and Mn(II)), X is an anionic ligand (NCS^-, NCO^-, CN^-, NO_3^- or halide), L is a substituted pyridine or α-arylalkylamine, and G is a guest, usually an organic aromatic compound. They have the ability to absorb organic compounds reversibly, and the first experimental studies of this phenomenon were carried out by Schaeffer and co-workers in 1957.[1] Lipkowski has studied various physico-chemical aspects of these compounds, including their selectivity, crystal structures, and the thermodynamics of sorption and kinetics of desorption, and these have been summarised in reviews.[2,3] In the well-studied Werner complex $[Ni(NCS)_2(4\text{-methylpyridine})_4]$ the two anionic ligands are in *trans* positions to each other and steric hindrance between the pyridine ligands results in a 'four-blade propeller' arrangement around the central metal ion. Noted in these studies is the dependence of lattice expansion on the volume and shape of the guest molecules. In most cases the host : guest ratio is 1 : 1. Physical properties of these structures are dependent on both the packing of the hosts as well as the kind of properties of the guest. The enthalpy of clathration is related to the cavities in the host lattice.[3] Soldatov[4] revisited the host compound $[Ni(NCS)_2(4\text{-methylpyridine})_4]$ and determined three crystal structures: dense (α), microporous (β) polymorphs and γ-inclusion phases. The adaptability of this host towards guest compounds is attributed to the fact that its β-phase volume expands by 5–14% upon guest inclusion. Recently there has been renewed interest in Werner clathrates[5,6] and Lusi and Barbour[7] have described polymorphism associated with an order–disorder phase transition of the guest in the $[Ni(NCS)_2(4\text{-phenylpyridine})_4]$ clathrate dependent on the thermal range investigated. The host preferentially discriminated in favour of one of the three isomers of xylene in solid–vapour competition experiments[8] and Batisai and co-workers[9] explored the preparation of phases by mechanochemical techniques which resulted in a series of solid solutions. Different sorption properties were exhibited by these solid solutions compared with the pure Werner complexes. Recently the structures of three Werner complexes have been analysed in terms of their packing, and the results of crystal densities were justified by Hirshfeld surface analysis and density functional theory calculations.[10]

In this work we present the structures, thermal decomposition kinetics and the selectivity of the Werner host $[Ni(NCS)_2(iso\text{-}quinoline)_4$, **H**] with *para*-, *meta*- and *ortho*-xylene (**px**, **mx** and **ox**, respectively). The ligand isoquinoline has a fused ring structure which according to the Cambridge Structural Database[11] has previously been encountered only once as a ligand in Werner clathrates[12] but its selectivity was not investigated. This ligand was chosen because its two fused rings give it a large aromatic surface area which is important for C–H···π and π···π host–guest interactions. The structural line diagrams and atomic numbering scheme for the **H** and the xylene guests are shown in Scheme 1.[13]

[a]*University of Cape Town, Rondebosch, Cape Town, South Africa. Fax: +27 21 6505419; Tel: +27 21 6505893*
[b]*Cape Peninsula University of Technology, Zonnebloem, Cape Town, South Africa. E-mail: bathorin@cput.ac.za; Tel: +27 21 4608354*

†Electronic supplementary information (ESI) available: The non-isothermal TG curves for **H·mx** and **H·ox** and the activation energies for **H·mx** and **H·ox**. CCDC 1041252–1041254. For ESI and crystallographic data in CIF or other electronic format see DOI: 10.1039/c5dt00084j

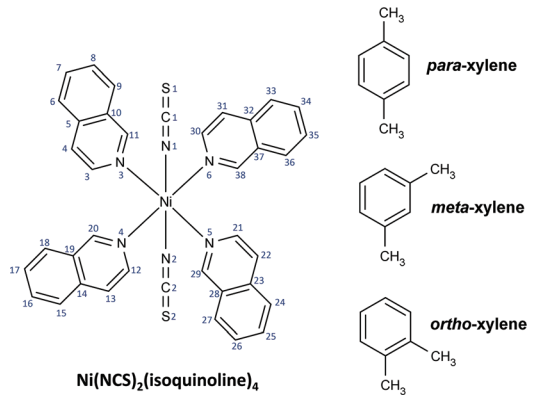

Scheme 1 Structural line diagrams and atomic numbering scheme of the host, $Ni(NCS)_2(isoquinoline)_4$, and the xylene isomers.

Results and discussion

Crystal structures of H·px, H·mx and H·ox

The structure of **H·px** was solved in the hexagonal space group $P6_1$ (no. 169) and the details of the data collection and refinement are summarised in Table 1. The asymmetric unit consists of one host and one guest molecule (Fig. 1a). The host is positioned in Wyckoff position a and is severely disordered. Two of the isoquinoline ligands lying *trans* across the Ni centre are disordered and eventually were modelled with 50% site occupancy. The final model of the ligand had refined the C and N atoms anisotropically and the H atoms with the usual riding model. The other two isoquinoline ligands and the thiocyanate groups were ordered and refined uneventfully. The atomic positions of the **px** guest were located unequivocally from the difference electron density map. However, convergence of the refinement could only be achieved with the guest treated isotropically with appropriate bond length constraints. The ordered **px** molecules are situated in cavities (Fig. 1b, **px** is presented with the space fill model, red) and form a helical arrangement along the *c* axis.

The **H·mx** structure displays similar features with the **H·px** and crystallised in the $P6_5$ (no. 170) space group. The asymmetric unit contains one host and one guest and the host positioned in Wyckoff position a. In a similar manner to **H·px**, the host has two ordered and two disordered isoquinoline ligands which were refined to 50% S.O.F.s (Fig. 1c). The **mx** guest is ordered and positioned in cavities (Fig. 1d) and the packing is enantiomeric with **H·px**.

The structure of **H·ox** was solved in the monoclinic *C*2/*c* (no. 15) space group. One host molecule is in the general position (Wyckoff f) and one is located in a diad (Wyckoff e). Similarly one guest is in the general position and the second guest is at the centre of inversion (Wyckoff b), thus the asymmetric unit is composed of 1.5 host and 1.5 guest molecules (Fig. 1e). The host molecule in the general position has one of its four isoquinoline ligands disordered and refined to S.O.F.s 77% and 23%. The host molecule is in a special position with two of its ligands situated on a diad. Both the ordered (Fig. 1f, molecule A, yellow) and the disordered guest (Fig. 1f, molecule B, green) are located in cavities. The structure shows remarkable similarity with **H·px** and **H·mx** from the [100] direction.

The intermolecular interactions between the xylene guests and the host framework were analysed using the program

Table 1 Crystallographic data for H·px, H·mx and H·ox

	H·px	H·mx	H·ox
Chemical formula	$Ni(NCS)_2(C_9H_7N)_4{\cdot}C_8H_{10}$	$Ni(NCS)_2(C_9H_7N)_4{\cdot}C_8H_{10}$	$Ni(NCS)_2(C_9H_7N)_4{\cdot}C_8H_{10}$
Host : guest ratio	1 : 1	1 : 1	1 : 1
Formula weight	797.65	797.65	1199.50
Temperature/K	173(2)	173(2)	173(2)
Crystal system	Hexagonal	Hexagonal	Monoclinic
Space group (no.)	$P6_1$ (no. 169)	$P6_5$ (no. 170)	*C*2/*c* (no. 15)
a/Å	10.7810(15)	10.8390(15)	10.671(2)
b/Å	10.7810(15)	10.8390(15)	19.132(4)
c/Å	59.780(12)	59.167(12)	59.609(12)
α/°	90.00	90.00	90.00
β/°	90.00	90.00	91.49(3)
γ/°	120.00	120.00	90.00
V/Å^3	6017.3(17)	6019.9(17)	12166(4)
Z′/*Z*	1/6	1/6	1.5/12
$D_{calc.}$/Mg m^{-3}	1.321	1.320	1.310
Radiation type	MoKα	MoKα	MoKα
F(000)	2496	2466	2016
Crystal size/mm	0.41 × 0.45 × 0.51	0.24 × 0.26 × 0.53	0.080 × 0.190 × 0.340
Colour, crystal form	Blue, octahedral	Blue, octahedral	Blue, octahedral
No. of total reflections	8794	5150	9660
No. of unique reflections	7094	4048	7315
$\Theta_{min-max}$/°	2.04/27.12	12.00/26.89	2.13/27.26
$R[F^2 > 2\sigma(F^2)]$, w$R(F^2)$, *S*	0.0692, 0.1963, 1.017	0.0461, 0.1055, 1.028	0.0686, 0.1639, 1.061
No. of parameters/data	637/8794	667/5150	893/9660
Res. peak (max/min)/e Å^{-3}	1.0102/−0.723	0.229/−0.166	0.796/−0.622

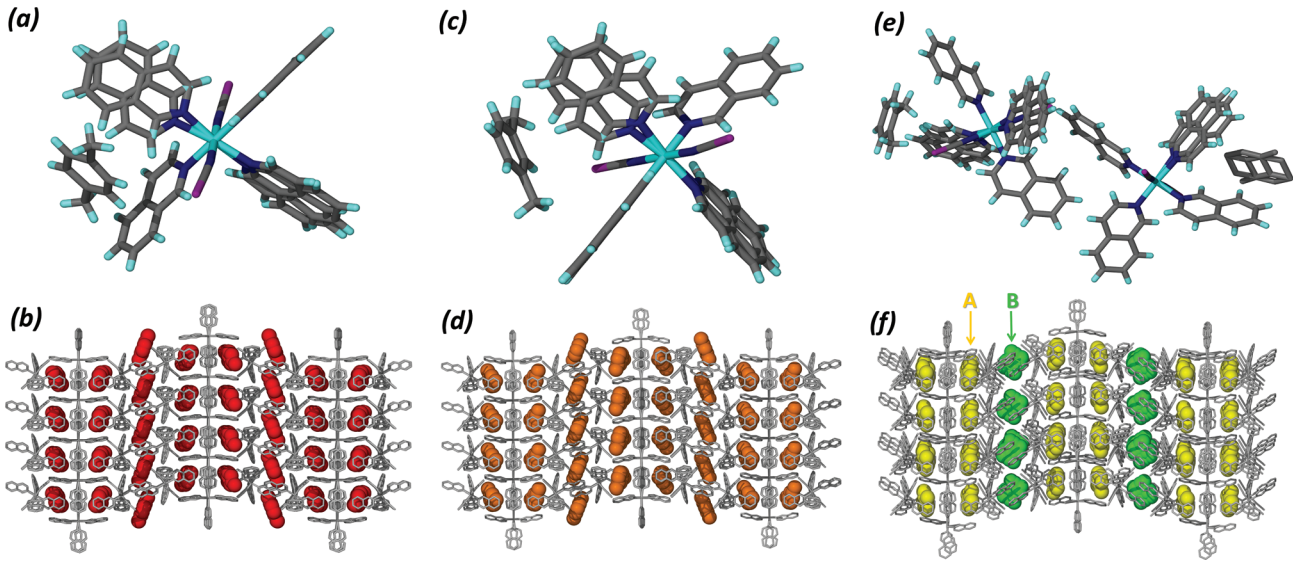

Fig. 1 Structural comparison of **H·px** ((a) molecular structure, (b) packing viewed down *a*, **px** is presented with the space fill model, red), **H·mx** ((c) molecular structure, (d) packing viewed down *a*, **mx** is presented with the space fill model, orange) and **H·ox** ((e) molecular structure, (f) packing viewed down *a*, **ox** is presented with the space fill model, yellow and green).

Crystal Explorer[14] which calculates the Hirshfeld surface[15] of a target molecule in a crystal structure and depicts all its interactions with the neighbouring molecules. Fig. 2a shows the **px** guest covered by its Hirshfeld surface when surrounded by host molecules and the generated fingerprint plot,[16] the 2D representation of the 3D surface. The red areas on the surface indicate C–H···π close contacts between the **px** and the hosts. The fingerprint plot was generated using one pair of the two disordered isoquinoline moieties. The resulting plot, generated by using the alternative pair of ligands, is very similar. The C···H contacts are highlighted in blue, and comprise *ca.* 48% of the interactions. The upper lobe, labelled ①, represents close contacts between the **px** hydrogens and the aromatic system of the host, while the lower lobe ② shows the contacts between the hydrogens of the ligands and the aromatic region of the **px**. The structure also displays a number of C–H···π interactions between the host molecules. Fig. 2b displays the **mx** guest in its Hirshfeld surface and the corresponding fingerprint plot shows a similar environment for the guest to the **H·px** structure with *ca.* 47% C···H contacts. In the

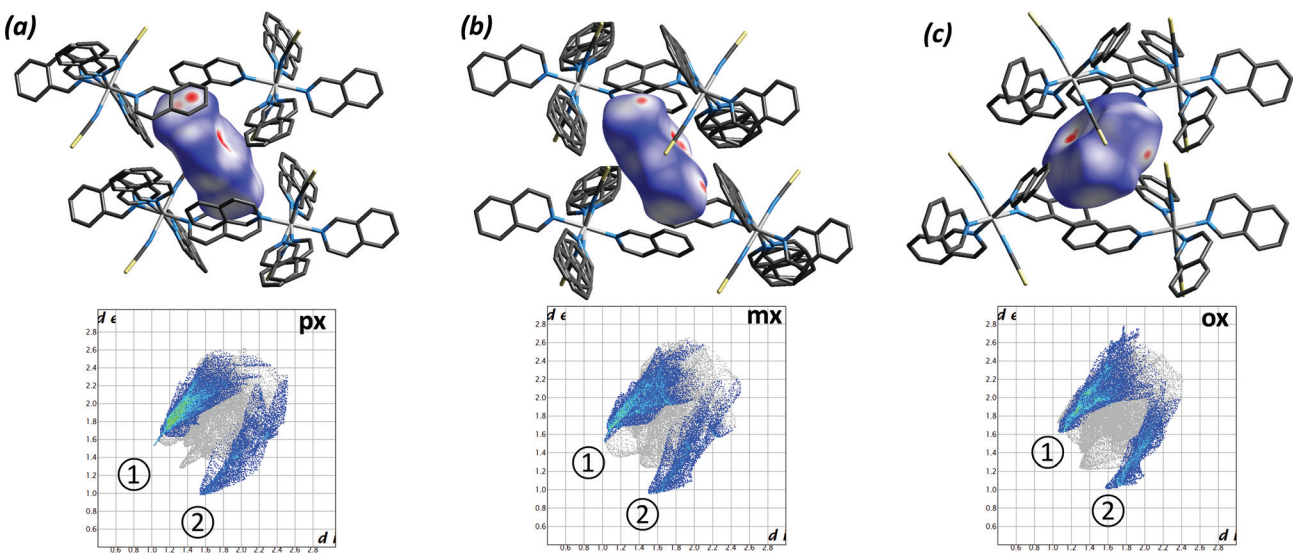

Fig. 2 Hirshfeld surfaces and their fingerprint plots of **px** (a), **mx** (b) and **ox** (c, ordered guest only); ① indicates close contacts between the guest hydrogens and the aromatic system of the host, while ② shows the contacts between the ligand hydrogens and the aromatic region of the guest.

case of **H·ox**, the disordered guest was not analysed. The Hirshfeld surface of the ordered guest shows less intensive interactions with the nearby hosts (smaller area in Fig. 2c). This corresponds to the amount of observed C···H contacts (*ca.* 44%) and their generally longer nature. Interestingly there are significant (**ox**)C–H···S(host) contacts with $(d_i + d_e)$ = 2.7 Å. This type of hydrogen bonding has previously been identified by Đaković *et al.* in Ni(II) complexes.[17]

Kinetics of thermal decomposition

The kinetics of thermal decomposition of all three inclusion compounds were carried out by the non-isothermal technique of Flynn and Wall.[18] Desorption curves were recorded at fixed heating rates β = 2, 4, 8, 16 and 32 K min^{-1} for all three clathrates. A set of curves for **H·px** is shown in Fig. 3. The decomposition takes place in three distinct steps. Step 1 represents the disintegration of the inclusion compound *via* loss of the guest. This step is calculated as a 13.3% loss in mass. Steps 2 and 3 correspond to the decomposition of the host, in each step the mass loss of two isoquinoline ligands at a percentage loss of 32.4% each. The decomposition curves of **H·mx** and **H·ox** are similar and have been deposited in the ESI (Fig. S1 and S2†). The calculated and experimental TG results for **H·px**, **H·mx** and **H·ox** are summarised in Table 2.

For Step 1 the mass loss corresponding to the loss of 1 mole of guest and activation energy were calculated over α ranges for each of the three inclusion compounds and are indicated in Table 3. The extent of reaction is defined as

$$\alpha = (m_t - m_0)/(m_\infty - m_0)$$

with m_0 = initial mass, m_t = mass at time t and m_∞ = final mass. Plots of $\log \beta/\beta_0$ *vs.* $1/T$ for the **H·px** where β is the heating rate are shown in Fig. 4. The activation energies for α positions 0.2, 0.5 and 0.75 of Step 1 are illustrated in Fig. 4a. Similarly, Step 2 at α positions 0.2, 0.5 and 0.8 and Step 3 at α positions 0.3, 0.45 and 0.6 are demonstrated in Fig. 4b and 4c, respectively. Activation energies were calculated from the slopes:

$$\text{slope} = -0.457\frac{E_a}{R}$$

The activation energies of the three thermal decomposition steps for each compound are shown in Table 3. Graphical information for **H·mx** and **H·ox** has been deposited in the ESI (Fig. S3 and S4†).

Step 1 decomposition reaction required the largest activation energy. The activation energy for Step 2 is the lowest of the three steps and is 105–108 for **H·px**, 103–116 for **H·mx** and 93–100 kJ mol^{-1} for **H·ox**. The higher values of the activation energies associated with the loss of the volatile xylene guests can be justified in terms of the topologies of the structures of the clathrates. In each case the xylene guest is trapped in a cavity, thus requiring a severe disruption of the host framework in order to release the guest. The effect of topology on the thermal stability and kinetics of decomposition of

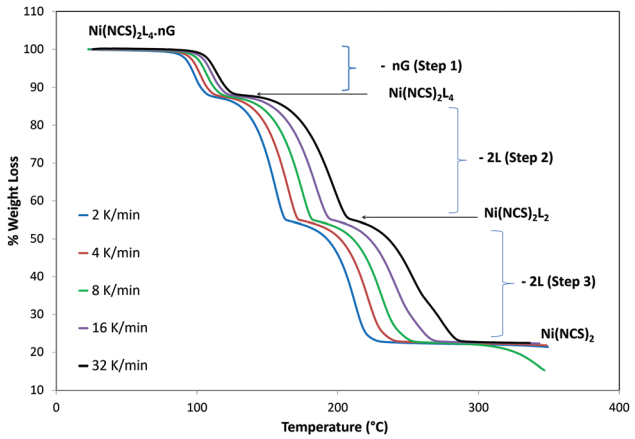

Fig. 3 Non-isothermal TG curves for H·px.

Table 2 Thermal analysis results for H·px, H·mx and H·ox

Compound	**H·px** exp (calc.) %	**H·mx** exp (calc.) %	**H·ox** exp (calc.) %
Mass loss			
Step 1	13.1 (13.3)	13.1 (13.3)	13.2 (13.3)
Step 2	32.3 (32.4)	32.1 (32.4)	31.8 (32.4)
Step 3	32.1 (32.4)	31.8 (32.4)	32.1 (32.4)

Table 3 Activation energy ranges for thermal decomposition (kJ mol^{-1})

Reaction step	**H·ox**	**H·mx**	**H·px**
Step 1	138–142	170–177	178–192
Step 2	93–100	103–116	105–108
Step 3	112	118–120	115–120

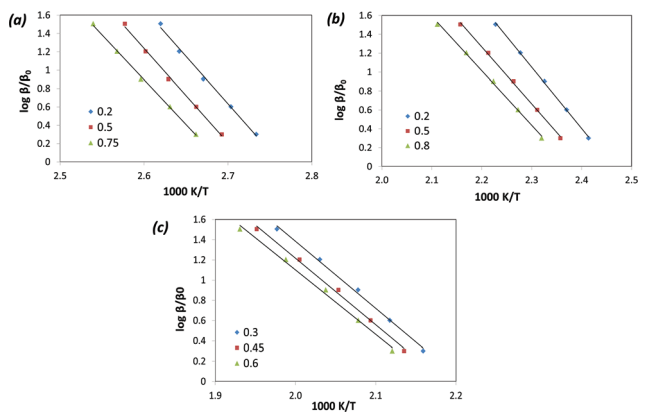

Fig. 4 Activation energies for (a) Step 1, (b) Step 2 and (c) Step 3 for H·px.

inclusion compounds has been reviewed[19] and, in general, structures that may be described as intercalates are less stable than tubulates, which in turn are less stable than cryptates. The latter often have higher activation energies of desorption.

Selectivity experiments

Experiments to determine the selectivity profile of this host were carried out by two methods. Firstly by dissolving the host in liquid mixtures of the guests with known proportions and harvesting the crystals of the ensuing inclusion compounds for analysis; secondly by exposing the powdered apohost to mixtures of the guest vapours (solid–vapour sorption) and subsequent analysis by headspace gas chromatography. These competition experiments between pairs of xylene isomers (**ox**/**px**, **ox**/**mx** and **mx**/**px**) were performed at different ratios (0 : 1; 0.2 : 0.8; 0.4 : 0.6; 0.6 : 0.4; 0.8 : 0.2 and 1 : 0). The crystals were harvested, dried and lightly crushed for analysis.

When a host compound is crystallised from a mixture of two guests A and B to form a crystal containing a ratio of the two guests (H·n′A·m′B), the selectivity coefficient of this competition experiment can be determined from the formula

$$K_{A:B} = (K_{B:A})^{-1} = Z_A/Z_B \times X_B/X_A \quad (X_A + X_B = 1)$$

where X_A and X_B are the mole fractions of the guests in the mother liquor and Z_A and Z_B are their mole fractions in the crystal. The results of the competition experiments are shown in Fig. 5 in which the mole fraction of a given guest in solution (X_{guest}) is plotted against its mole fraction in the solid state (Z_{guest}). In Fig. 5a a small amount of preference is shown for **ox** over **px** for the composition mixture of **ox**/**px**. Fig. 5b indicates the selectivity of **ox** compared with **mx** in the crystal structure with the host showing no preference for one over the other. Similarly in Fig. 5c there is no preference for the host to enclathrate one of **mx** or **ox** over the other. Selectivity for both procedures (crystallisation and solid–vapour sorption) is shown graphically and no preference for either of the two xylenes is observed. That is, in all the three cases poor selectivity is found for one of the isomers over the other two.

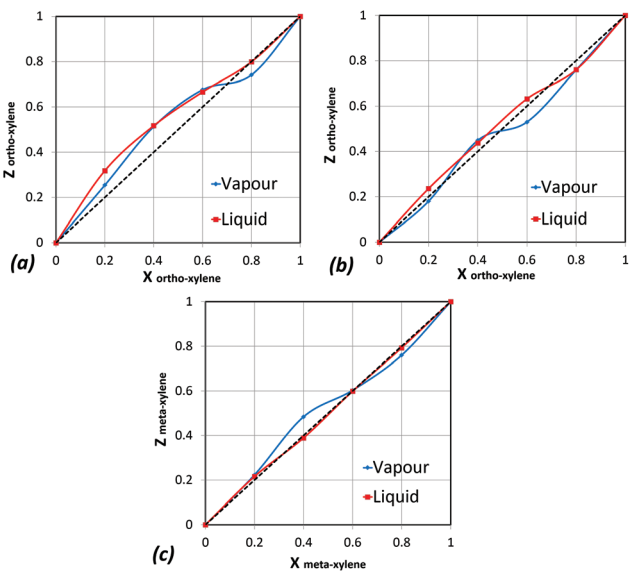

Fig. 5 Selectivity curves for (a) **ox**/**px**; (b) **ox**/**mx** and (c) **mx**/**px**.

Discussion

The question to be addressed is why the isoquinoline host under discussion is not selective towards any of the xylene isomers either from liquid or vapour mixtures, while the host bis(isothiocyanato)tetrakis(4-phenylpyridine)nickel(II) has been shown to discriminate efficiently between *ortho*-, *meta*- and *para*-xylenes.[8] Competition experiments between equimolar pairs of two isomers and an equimolar mixture of all three xylenes in the vapour state show the preference for enclathration to be in the order **ox** > **mx** > **px**. We have therefore analysed the non-bonded interactions which occur between a given guest and this host. We have chosen to compare the structures containing the *ortho*- and *meta*-xylene guests, because they are similar in that they both have a host : guest ratio of 1 : 1, while the structure of *para*-xylene has a host : guest ratio of 1 : 3. The program Crystal Explorer was employed to calculate the Hirshfeld surfaces of the **ox** and **mx** molecules and their fingerprint plots were generated (Fig. 6).

Fig. 6a shows the fingerprint plot of the **ox** guest. The two peaks labelled ① are associated with H···H interactions at (d_i + d_e) ≈ 2.48 Å (57% of the close contacts) while those labelled ② are due to C···H contacts with (d_i + d_e) ≈ 2.87 Å (37%). In contrast, the **mx** structure, shown in Fig. 6b, has H···H contacts labelled ① at 2.43 Å (68%) and C···H contacts labelled ② at 2.85 Å (28%). The Hirshfeld surface analysis supports the experimental results and explains why the host favours the **ox** guest. Also it demonstrates that the H···H and C···H interactions occur at similar distances, slightly over the sum of the van der Waals radii of 2.40 and 2.90 Å[20] respectively, but there is a greater percentage of C···H interactions in the **ox** structure and the circled area in Fig. 6b shows that there are many long H···H contacts, resulting in a less efficient packing of the **mx** structure.

In addition to the host–guest non-bonded interactions, however, the host with 4-phenylpyridine ligands possesses

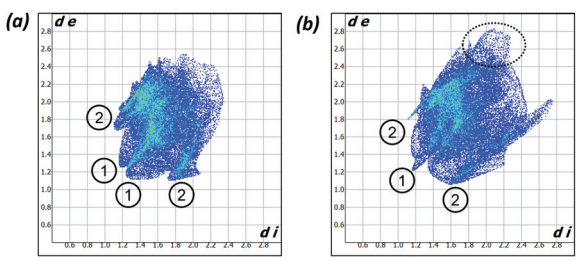

Fig. 6 Fingerprint plots for (a) the **ox** guest and (b) the **mx** guest in their inclusion compounds with bis(isothiocyanato)tetrakis(4-phenylpyridine) nickel(II).

considerable torsional flexibility in its pyridine and phenyl rings. This fact has been discussed in detail previously.[21] The labelling of the four torsion angles (τ_1, τ_3, τ_5 and τ_7) between the pyridine ring and the thiocyanato ligand (N–Ni–N–C) was carried out cyclically in a manner to yield the minimum in the sum of the square of their differences. The eight torsion angles of each of the three structures have been tabulated and labelled as before[21] (Fig. 7) and their values are summarized in Table 4. It was noted that the differences in the torsion angles τ_3 and τ_4 as well as τ_7 and τ_8 observed in the **mx** structure indicated large rotations of the phenyl ring (Table 4 for **mx**, Δ values in bold) compared with τ_1/τ_2 and τ_5/τ_6 differences. The selectivity for **mx** is less than **ox** but greater than **px**. In the case of **ox**, alternating positive and negative torsion rotations are observed (τ_1/τ_2 and τ_5/τ_6 negative; τ_3/τ_4 and τ_7/τ_8 positive). This attests the fact that this is a highly flexible ligand, which easily adapts to the requirement of a given guest, rendering it selective.

The torsion angles describing the pyridine moieties in the currently investigated host **H** (τ_1, τ_3, τ_5 and τ_7) are remarkably similar to previously analysed compounds. They correspond to the 'four-blade propeller' configuration found in the structures of analogous compounds containing pyridine (**W1**), 4-methyl- (**W2**), 4-vinyl- (**W3**), and 4-phenyl- (**W4**) pyridines. This corresponds to the ++++ configuration described by Lipkowski.[2,22] Table 5 and Fig. 8 show the range of torsion angles for these

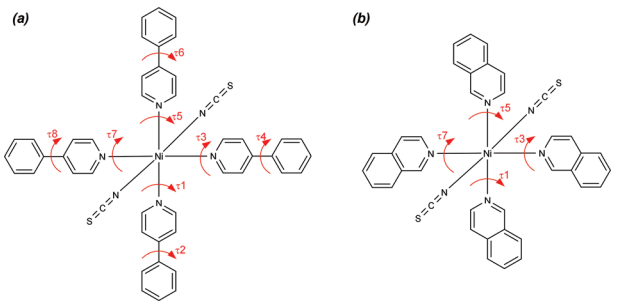

Fig. 7 Torsion angles in (a) $Ni(NCS)_2(4\text{-phenylpyridine})_4$ and (b) **H**.

Table 4 Torsion angles of $Ni(NCS)_2(4\text{-phenylpyridine})_4$ in its crystals of xylene isomers

Guest	τ_1/τ_2	τ_3/τ_4	τ_5/τ_6	τ_7/τ_8
Ox	32.4	39.7	34.1	43.9
	45.1	25.7	44.4	31.3
Δ	−12.7	14.0	−10.3	12.8
mx	20.3	20.8	46.6	34.4
	21.8	−29.7	15.5	−30.1
Δ	−1.5	**50.5**	31.1	**64.5**
px	23.0	34.6	40.2	39.7
	34.7	19.2	40.0	27.1
Δ	−11.7	15.4	0.2	12.6

Table 5 Torsion angles τ_1, τ_3, τ_5 and τ_7 for **H** and some typical nickel Werner clathrates where the ligands are pyridine (**W1**), 4-methyl- (**W2**), 4-vinyl- (**W3**), and 4-phenyl- (**W4**) pyridine

Compound	τ_1 (°)	τ_3 (°)	τ_5 (°)	τ_7 (°)
H·px	16.5	49.9	17.9	50.3
H·mx	24.5	25.1	48.3	50.3
H·ox	24.2	50.8	26.4	59.3
W1	15.7	21.6	51.6	34.5
W2	30.4	39.8	35.7	40.6
W3	33.3	36.8	44.5	38.5
W4	29.2	36.0	43.9	48.0

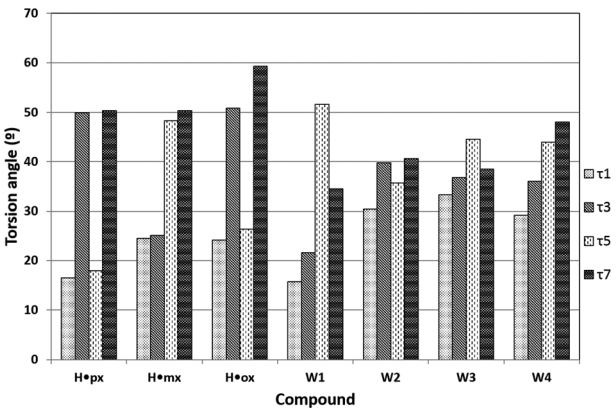

Fig. 8 Plot of torsion angles of Werner complexes based on values presented in Table 5.

apohosts, as well as the torsion angles for the currently discussed three structures **H·px**, **H·mx** and **H·ox**. Despite presenting four positively rotated ligands in the isoquinoline host **H**, the torsion angles also indicate two large and two smaller angles. This shows compensation for the interaction of the host with the guest, whereas in the apohost structures no guest is present.

Experimental section

Preparation of Werner clathrate

The host compound, **H**, bis(isothiocyanato)tetrakis(isoquinoline)nickel(II), was prepared by adding stoichiometric quantities of an ethanolic solution of isoquinoline (20 ml, 0.01 M) to an ethanolic solution of nickel isothiocyanate (5 ml, 0.01 M). Violet crystals of $Ni(NCS)_2(C_9H_7N)_4$ were formed immediately and were filtered and allowed to air dry overnight.

Enclathration of any given xylene guest was carried out by dissolving the host in benzene, adding the xylene isomer (**px**, **mx** and **ox**) dropwise and stirring at 60 °C for 30 minutes, cooling and filtering. Crystallisation occurred within 24 hours. Deep blue crystals of **H·px**, **H·mx** and **H·ox** were formed.

Single crystal X-ray analysis

Intensity data of a selected single crystal for compounds **H·px**, **H·mx** and **H·ox** were collected on a Bruker DUO APEX II diffractometer[23] with graphite monochromated Mo $K_{\alpha 1}$ radiation (λ = 0.71073 Å) at 173 K using Oxford Cryostream 700. Data reduction and cell refinement were performed using Saint Plus.[24] The space group was determined from systematic absences by using XPREP.[25] The structure was solved using SHELXS-97[26] and refined using full matrix least squares methods in SHELXL-97[28] with the aid of the program X-Seed.[27] The hydrogen atoms bound to carbon atoms were placed at idealized positions and refined as riding atoms. Diagrams and publication material were generated using PLATON,[28] X-Seed and Mercury (3.1).[29] Crystal data and structure refinement parameters are given in Table 1. CCDC 1041252–1041254 contain the supplementary crystallographic data for structures **H·px**, **H·mx** and **H·ox**.

Powder X-ray diffraction

Powder X-ray diffraction experiments were carried out on a Bruker D8 diffractometer using Cu K_{α} radiation. The sample was ground to a fine powder and loaded into an aluminium tray. Where available these spectra were compared with those determined from the single crystal structures.

Thermogravimetric analysis

Thermal analyses were performed on a TA Q500 instrument from 30 to 350 °C at heating rates ranging from 2, 4, 8, 16 and 32 °C min^{-1} with dry nitrogen as purge gas flowing at 60 ml min^{-1}. All samples were dried on filter paper and placed in an open pan for thermogravimetric analysis. Sample masses varied from 2 to 5 mg.

Competition experiments

The selectivity of the host for a particular isomer was evaluated using two different procedures and analysing both by headspace gas chromatography. The first was a solid–vapour experiment in which the crushed host was exposed to a mixture of two xylene guests in an evacuated chamber at room temperature for 18 hours. The compound was removed from the chamber, dried and placed in a headspace vial for GC analysis. The second method involved crystal formation of the host with a guest mixture using the same procedure mentioned above. Crystals were harvested, dried and placed in headspace vials for GC analysis.

Gas chromatography

GC analysis was performed on an Agilent 7890A instrument with a Varian CP Wax capillary column (30 m × 250 μm × 0.25 μm), nitrogen carrier gas and FID detector with inlet and detector temperatures of 280 °C. Vials were incubated at 50 °C for 10 minutes before injection; oven temperature at 35 °C for 1 minute, followed by a gradient at 10 °C min^{-1} to 120 °C for 2 minutes.

Conclusions

A Werner clathrate $[Ni(NCS)_2(isoquinoline)_4]$ has been synthesised and its properties were elucidated. Due to the importance of the xylene isomers in the petroleum industry, *para*-, *meta*- and *ortho*-xylenes were considered as the guests in this study. Single crystal structures of the host·guest compounds were analysed and the packing was established. The analysis of the fingerprint plots revealed the importance of the C–H···π interactions and unique C–H···S interactions were observed in the **H·ox** structure.

The non-isothermal technique of Flynn and Wall was used to record the kinetics of thermal decomposition of the three inclusion compounds. Similar plots for the three compounds show initial loss of the guest, followed by two steps, each denoting the mass loss of two isoquinoline ligands.

The selectivity of **H** towards the xylene isomers was determined using two methods, *viz*. solid–vapour sorption and crystallisation from a liquid solution of the host and a bimolecular mixture of the guests. The results were analysed using headspace gas chromatography. No significant preference for one of the xylene isomers over the other two was found, showing poor selectivity of this host.

The poor selectivity of this host **H** was compared to that of the related host $[Ni(NCS)_2(4\text{-phenylpyridine})_4]$. The success of the latter host was attributed to the torsional flexibility of the phenyl moieties in the ligands. In contrast, the isoquinoline ligands, although containing larger aromatic systems, have no such flexibility and their relative conformation is largely controlled by their *ortho*-hydrogens.

Acknowledgements

Authors thank Mr David Kok for assistance with the GC analysis, Dr Eustina Batisai, the National Research Foundation (Pretoria, South Africa) and the Cape Peninsula University of Technology for financial support. The authors declare that they have no conflict of interest.

Notes and references

1 W. D. Schaeffer, W. S. Dorsey, D. A. Skinner and C. G. Christian, *J. Am. Chem. Soc.*, 1957, **79**, 5870.
2 J. Lipkowski, in *Inclusion Compounds*, Academic Press, New York, 1984, vol 1, ch. 3.
3 J. Lipkowski, in *Comprehensive Supramolecular Chemistry*, ed. D. D. MacNicol, F. Toda and R. Bishop, Elsevier Science, Oxford, 1996, vol. 6, ch. 20.
4 D. V. Soldatov, G. D. Enright and J. A. Ripmeester, *Cryst. Growth Des.*, 2004, **4**, 1185.
5 C. J. Adams, M. F. Haddow, D. J. Harding, T. J. Podesta and R. E. Waddington, *CrystEngComm*, 2011, **13**, 4909.
6 S. Wohlert, I. Jess, U. Englert and C. Nather, *CrystEngComm*, 2013, 5326.

7 M. Lusi and L. J. Barbour, *CrystEngComm*, 2014, **16**, 36.
8 M. Lusi and L. J. Barbour, *Angew. Chem., Int. Ed.*, 2012, **51**, 3928.
9 E. Batisai, M. Lusi, T. Jacobs and L. J. Barbour, *Chem. Commun.*, 2012, 12171.
10 S. M. Soliman, Z. B. Elzawy, M. A. M. Abu-Youssef, J. Albering, K. Gatterer, L. Öhrström and S. F. A. Kettle, *Acta Crystallogr., Sect. B: Struct. Sci.*, 2014, **70**, 115.
11 F. Allen, *Acta Crystallogr., Sect. B: Struct. Sci.*, 2002, **58**, 380.
12 P. Baran, M. Boča, R. Boča, A. Krutošíková, J. Miklovič, J. Pelikán and J. Tituš, *Polyhedron*, 2005, **24**, 1510.
13 MarvinSketch 14.8.11.0, 2014, ChemAxon (http://www.chemaxon.com).
14 S. K. Wolff, D. J. Grimwood, J. J. McKinnon, M. J. Turner, D. Jayatilaka and M. A. Spackman, *CrystalExplorer (Version 3.1)*, University of Western Australia, 2012.
15 M. A. Spackman and D. Jayatilaka, *CrystEngComm*, 2009, **11**, 19.
16 (*a*) M. A. Spackman and J. J. McKinnon, *CrystEngComm*, 2002, **4**, 378; (*b*) J. J. McKinnon, D. Jayatilaka and M. A. Spackman, *Chem. Commun.*, 2007, 3814.
17 M. Đaković, D. Vila-Viçosa, M. J. Calhorda and Z. Popović, *CrystEngComm*, 2011, **13**, 5863.
18 J. H. Flynn and L. A. Wall, *Polym. Lett.*, 1966, **4**, 323.
19 L. R. Nassimbeni, *Acc. Chem. Res.*, 2003, **36**, 631.
20 A. Bondi, *J. Phys. Chem.*, 1964, **68**, 441.
21 L. R. Nassimbeni, M. L. Niven and M. W. Taylor, *Inorg. Chim. Acta*, 1987, **132**, 67.
22 J. Lipkowski, *J. Mol. Struct.*, 1981, **75**, 13.
23 *Bruker 2005. APEX2. Version 1.0-27*, Bruker AXS Inc., Madison, Wisconsin, USA.
24 *Bruker 2004. SAINT-Plus (including XPREP). Version 7.12*, Bruker AXS Inc., Madison, Wisconsin, USA.
25 *Bruker 2003, XPREP2. Version 6.14*, Bruker AXS Inc., Madison, Wisconsin, USA.
26 G. M. Sheldrick, *SHELXS-97 and SHELXL-97 Programs for crystal structure determination and refinement*, University of Göttingen, 1997.
27 L. J. Barbour, *J. Supramol. Chem.*, 2001, **1**, 189.
28 A. L. Spek, *PLATON, A Multipurpose Crystallographic Tool*, Utrecht University, Utrecht, The Netherlands, 2008.
29 C. F. Macrae, I. J. Bruno, J. A. Chisholm, P. R. Edgington, P. McCabe, E. Pidcock, L. Rodriguez-Monge, R. Taylor, J. van de Streek and P. A. Wood, *J. Appl. Crystallogr.*, 2008, **41**, 466.